

Document downloaded from:

<http://hdl.handle.net/10251/75132>

This paper must be cited as:

Pastor Soriano, JV.; García Oliver, JM.; Nerva, J.; Giménez, B. (2011). Fuel effect on the liquid-phase penetration of an evaporating spray under transient diesel-like conditions. *Fuel*. 90(11):3369-3381. doi:10.1016/j.fuel.2011.05.006.



The final publication is available at

<http://dx.doi.org/10.1016/j.fuel.2011.05.006>

Copyright Elsevier

Additional Information

Fuel Effect on the Liquid-Phase Penetration of an Evaporating Spray Under Transient Diesel-like Conditions

J.V. Pastor^{a*}, J.M. García-Oliver^a, J.-G. Nerva^a, B. Giménez^b

^a *CMT-Motores Térmicos. Universitat Politècnica de València
Camino Vera s/n - 46022 Valencia, Spain.*

^b *Department of Energy and Fluid Mechanics Engineering. University of Valladolid.
Paseo del Cauce s/n, 47011 Valladolid, Spain.*

Abstract

Measurements of the maximum liquid-phase penetration have been performed injecting five different fuels through a single-hole nozzle in an optical engine under a large set of thermodynamic and injection conditions. The focus of this paper is twofold. First, it pretends to study fuel physical properties on liquid-phase fuel penetration. The choice made on Fischer-Tropsch diesel (*FTD*) and biodiesel fuels has been highly motivated by their potential to be, at short or middle term, possible substitutes to the conventional diesel fuel. Extensive characterization of fuel physical and chemical properties under ambient conditions are provided and related to the liquid-phase penetration in order to provide an accessible tool to predict liquid spray behavior based on cheap, off-engine measurements. Fischer-Tropsch fuels appeared to be the easiest to vaporize while biodiesel blends were getting always harder to vaporize as the Rapeseed Methyl Ester (*RME*) rate was increased. The second

*Corresponding author

Email address: jpastor@mot.upv.es (J.V. Pastor^a)

objective of this work is to study the time-response of liquid-phase penetration when subjected to density and temperature variations. Injections of 8 *ms* at three different pressures have been performed in transient diesel-like conditions with density and temperature time derivatives up to 2000 $kg.m^{-3}.s^{-1}$ and 20000 $K.s^{-1}$. In most cases, the spray appeared to closely follow predictions made from empirical models built out of steady-state air conditions, leading to the conclusion of an instantaneous adjustment of the spray to its environment, validating: (1) the hypothesis made in 1D spray models; (2) the use of empirical models in unsteady-state environment when obtained under steady-state conditions.

Key words: diesel engine, biodiesel, spray, Fischer-Tropsch, fuel properties, liquid length, correlation, unsteady conditions.

1. Introduction

During the past two decades, research on the effect of fuel properties may not have received fervent interest by the automotive industry, perhaps due to the long-standing establishment of conventional diesel and the lack of viable alternative solutions. Although the studies available on the subject represent precious information for the validation of spray modeling hypothesis [1, 2, 3, 4], most of the research effort has been channeled into new combustion concepts using complex injection strategies and high *EGR* levels in order to reduce both NO_X and PM . More recently, worldwide environmental agencies have been inciting car constructors to find alternatives to the exhaustible fossil fuel for a better sustainability of energy management [5]. In this ambitious framework, biofuels and synthetic fuels represent an

13 interesting perspective, at least at short and middle term, for their capac-
14 ity to be directly implanted in the actual car park with no major change
15 of the engine design. Their effect on combustion efficiency and emissions
16 is the result of a complex succession of physical and chemical processes [6].
17 This study pretends to understand and assess which are the physical mech-
18 anisms involved in the introduction of alternative fuels. For this objective,
19 various off-engine measurements have been performed on the five fuels be-
20 fore their injection through a $82\ \mu\text{m}$ -single-hole nozzle, in an optical engine
21 [7] fed with pure nitrogen. The visualization of their respective maximum
22 liquid-phase penetration has been realized under a large set of operating con-
23 ditions, including a sweep of air temperature at constant density, a sweep of
24 air density at constant temperature and three different injection pressures
25 have been performed for each fuel. High-speed imaging of the spray shadow
26 left on a highly lit background has been processed to measure the maximum
27 liquid-phase penetration as defined by Dec and Siebers in [9, 10]. In the first
28 instance, liquid length results and air conditions have been time-averaged as
29 in [11, 12, 13] and discussed. In a second instance, unsteadiness of air den-
30 sity and air temperature during the fuel injection has been used as a way to
31 increase the number of experimental data and consequently the reliability of
32 statistics. For each image and so for each instant of the $8\ \text{ms}$ injection event,
33 its corresponding air temperature and density were associated. Apart from
34 presenting clear advantages on the statistical point of view [14], these results
35 permitted to conclude on spray reactivity when submitted to variations of
36 ambient density and temperature.

37 2. Experimental Setup

38 2.1. Fuels

39 Five different fuels have been selected for their capacity and their poten-
40 tial to be used in a diesel engine with no fundamental redesign of the engine
41 whilst having significant differences in both physical and chemical properties.
42 The first three fuels are widely known in the literature under the generic la-
43 bel "first generation biodiesels". Indeed, they are partially or entirely issued
44 from cereal feedstock. *RME* (Rapeseed Methyl Ester) is a fuel issued from
45 the transesterification reaction between rape oil and methanol. *B05* and *B30*
46 are blends of fossil diesel with respectively 5 and 30 mass percentage of the
47 same *RME*.

48 [Table 1 about here.]

49 These three fuels have been previously used by the authors in a multi-hole
50 injector configuration under both reactive and non-reactive environments
51 [12, 13]. Finally, the two last fuels are Fischer-Tropsch fuels issued from gas,
52 coal or biomass liquefaction and will be referred as *FT1* and *FT2* in the fol-
53 lowing study. Various measurements of fuel properties have been performed
54 off-engine. Thermodynamic properties, energetic content and equivalent for-
55 mula have been measured following *ASTM* standards and are summarized
56 in Table 2. Results show that by increasing *RME* rate in biodiesel fuels,
57 both density and viscosity increase as well, whereas *LHV* reduces because
58 of the increasing oxygen content. Both Fischer-Tropsch fuels have a lower
59 density compensated by a higher energetic content, which is an important
60 data under a marketing point of view, since the energetic content of one

61 liter is pretty much the same between all these fuels. *FT2* is singular by its
62 very low viscosity and its small extra oxygen content. Comparative trends
63 in fluid-mechanics properties were also observed in [15] for a similar selec-
64 tion of fuels. Chemical equivalent formulas have been measured using gas
65 chromatography-FID and are also provided in Table 1. They appear to be
66 close to heptadecane ($C_{17}H_{36}$) and dodecane ($C_{12}H_{26}$) formulas respectively
67 for *FT1* and *FT2* while *RME*'s closest pure surrogate could be methyl-oleate
68 ($C_{19}H_{36}O_2$). Distillation curves have been measured under the *ASTMD86*
69 standard. Besides, a weighing scale was measuring the collected mass simul-
70 taneously, in order to detect a possible shift between mass and volume recov-
71 ery percentage. Results are presented in Figure 1. On one hand, *RME* and
72 *FT2* appear to have relatively flat distillation curves, which is the witness of
73 their homogeneity and their similitude to their corresponding surrogate. On
74 the other hand, *B05*, *B30* and *FT1* have similar trends in evaporation under
75 atmospheric pressure, starting from values close to *FT2* and ending to values
76 close to *RME*. Consequently, it can be expected that *B05*, *B30* and *FT1*'s
77 lightest fractions are molecules heavier than *FT2* ($C_{12}H_{25}O_{0.2}$) and that their
78 heaviest fractions are close to *RME*'s molecular weight ($C_{18.95}H_{35.2}O_2$). For
79 *B05* and *B30*, their *RME* content is expected to correspond to this heavy
80 fraction. No significative differences can be observed on the comparison be-
81 tween mass and volume percentage recovery. This attests that no important
82 variations of density exist among the proper components of each fuel.

83 [Figure 1 about here.]

84 While the fuel was getting to the temperature of its first boiling point, an
85 important volume expansion has been observed, measured and traduced to

86 density as a function of temperature, considering mass conservation. Results
87 plotted in Figure 2 show linear trends with high R^2 . Coefficients for a linear
88 regression $\rho_f = B + A.T_f$ have been summarized in Table 2. *ASTM D1298*
89 measurements have been added to the plot as well for illustration, but have
90 not been used in the linear regressions for data consistency. A small offset
91 exists between the *ASTM* measurements and what would be the correspond-
92 ing measurement by volume at 289 K. Such volume measurements are not as
93 accurate as the *ASTM D1298* but authors believe that the trend is reliable
94 enough to be used as $\rho_f = \rho_{ASTMD1298} + A.(T_f - 289)$. It can be observed how
95 these coefficients (A) are all slightly inferior to the value for the US diesel #2
96 (0.9) referred by Siebers in [16].

97 [Figure 2 about here.]

98 [Table 2 about here.]

99 2.2. Hot Spray Test Rig

100 [Figure 3 about here.]

101 Tests have operated in a rapid cycling machine described in [7] and illustrated
102 in Figure 3. This facility is based on a modified loop-scavenged single cylin-
103 der 2-stroke direct injection diesel engine with three liter displacement and
104 low rated rotational speed (500 rpm). This apparatus makes optical studies
105 on free sprays under inert or reactive diesel-like thermodynamic conditions
106 possible. Intake and exhaust being handled by transfers on the liner, opti-
107 cal access to the high-pressure chamber can be easily achieved through the
108 cylinder head which encloses a cylindrical combustion chamber large enough

109 to avoid spray impingement against engine walls. This chamber has an up-
110 per port where a single-hole injector equipped with a $82\ \mu\text{m}$ conical nozzle
111 is mounted, and four lateral orthogonal accesses. One of these accesses is
112 used by a pressure transducer whereas the three other ones are equipped
113 with oval-shaped quartz windows, $88\ \text{mm}$ long, $37\ \text{mm}$ large, and $28\ \text{mm}$
114 thick. Although the use of a single-hole injector may produce faster pressure
115 build-up in the nozzle sac-hole, a faster needle lift and a higher pressure at
116 full needle lift [8], it still presented certain benefits compared to the multi-
117 hole one previously used by the authors in the same facility [12]. First, it
118 impeded spray-to-spray interaction (aerodynamic + thermodynamic) and its
119 position relative to the chamber allowed a much larger field for spray de-
120 velopment ($80\ \text{mm}$ vs. $35\ \text{mm}$). Above all, the mass injected was strongly
121 limited despite the performing of relatively long injections, so that no effect
122 on thermodynamic conditions alteration has been detected on the pressure
123 trace. Indeed, in [12], the use of a multi-hole injector with $130\ \mu\text{m}$ nozzle
124 hole had led the authors to consider the ambient temperature reduction due
125 to fuel vaporization energetic consumption. The window for time-averaging
126 had to be limited in order to consider steady-state environment. More de-
127 tails about the nozzle and injection settings can be found in Figure 4. For
128 this study, the inert configuration has been set by feeding the engine with
129 pure nitrogen so that any reaction due to air oxygen content was avoided.
130 Consequently, outcomes relative to this work concern exclusively the physi-
131 cal processes associated to fuel injection, atomization, mixing, heat transfer
132 and vaporization. The rig has been operated under a skip fire mode, i.e.
133 one injection event occurs every 20 engine cycles. This strategy is commonly

134 used to minimize windows fouling and to let the system filter the air and
135 then avoid air saturation with vaporized fuel.

136 [Figure 4 about here.]

137 2.3. Operating Conditions

138 [Figure 5 about here.]

139 The test matrix includes five different engine operating conditions which
140 have been selected in order to realize a sweep of three T_{max} at constant
141 ρ_{max} (26 kg.m^{-3}) and a sweep of three ρ_{max} at constant T_{max} (800 K) as
142 shown in Figure 5. The five operating conditions have been labeled *NO*,
143 *LT*, *HT*, *LD*, *HD*, standing respectively for NOminal, Low Temperature,
144 High Temperature, Low Density and High Density air setup. The five fuels
145 have been injected at three pressure levels (50, 100 and 150 *MPa*). The
146 injector was triggered at -16°ATDC and energized during 8 *ms* ($\approx 24 \text{CAD}$
147 depending on the instantaneous speed close to the TDC of each operating
148 condition). All information relative the the injector has been summarized
149 in Table 3. Each test has been repeated 10 times leading to a total number
150 of injections equal to 750 for the whole study (5 *fuels* x 5 *OC* x 3 P_{inj} x
151 10 *inj.*). To determine the exact intake air condition required by the test
152 plan, an accurate characterization of the engine has been performed over
153 35 points covering its full range of operating conditions. Thermodynamic
154 conditions have been calculated from the cylinder pressure using a first-law
155 thermodynamic analysis considering blow-by, heat transfer and mechanical
156 stress. By a succession of interpolations, the exact air intake conditions for
157 the test plan are then calculated. A double-check is performed by setting

158 the resulting values to the engine and the reiteration of the same first-law
159 analysis. Results of the engine characterization can be found in Table 3 and
160 intake conditions to carry out the test plan are indicated in Figure 5. The
161 resulting temperature and densities in the close to TDC region are plotted
162 in Figure 6.

163 [Figure 6 about here.]

164 [Table 3 about here.]

165 2.4. Optical Setup and Image Processing

166 Diffused back-light images have been taken at 8000 *fps*. Illumination was
167 provided by two 150 *W* quartz-halogen illuminators (Dolan-Jenner PL800),
168 supplied by 8 *mm* optic fiber bundles positioned at 60 *mm* from the diffuser
169 dispensing an illumination of 330 $W.m^{-2}$. The optical setup is represented in
170 Figure 3. Exposure time of the high-speed CMOS camera (Photron Fastcam-
171 Ultima APX) has been limited to 25 μs . Imaging has been kept to this
172 relatively low speed in order to keep a reasonable spatial resolution of 8.9
173 *pixels/mm*. Camera bit depth of 10 bits allowed a good discretization of
174 digital levels for subsequent image segmentation. The camera was triggered
175 by a *TTL* signal synchronized with the injector start of energizing (*SOE*).
176 Each injection event was documented by 100 pictures, accommodating a 12.5
177 *ms* acquisition time from the *SOE*.

178 Images of the spray have been processed with a purpose-made C++ code
179 described in [12, 17, 18]. Figure 8 shows two of these processing steps. After
180 a background subtraction (a), a threshold is calculated based on a statistical
181 analysis of each image background [12] and used for image segmentation.

182 Connectivity to the spray center of mass removes any imperfection left on
183 the segmented image. The distance between the injector tip and the front
184 part of the detected boundary is considered to be the maximum liquid-phase
185 penetration (b).

186 **3. Analysis Methodology**

187 As commented in the introduction, data have been processed in two dif-
188 ferent ways to assess physical processes associated to engine operation and
189 fuel physical properties. After a short theoretical review, the approach of the
190 statistical analysis and its relation to the experiment will be presented.

191 [Figure 7 about here.]

192 *3.1. Theoretical background*

193 The computational cost of *CFD* motivated investigation for the under-
194 standing and the assessment of the phenomena occurring in a diesel spray to
195 simplify the calculation of spray flow-field development. Thus, different 1D-
196 models have been proposed [16, 19, 23] based on mixing-limited vaporization
197 control, in which hypothesis made are the following: - The spray reaches the
198 complete atomization regime very near the nozzle exit. - Local transfer rates
199 of momentum, mass and energy between liquid droplets and surrounding air
200 are fast in comparison to the rate of development of the flow field as a whole.
201 This means that an a priori complicated two-phase problem is treated from
202 the point of view of a single-phase flow where a fraction of fuel vaporizes
203 instantaneously once there is enough enthalpy in the surrounding gas to heat
204 it up and vaporize it. The appropriate mixture fraction where this energy

205 balance is achieved is called $Y_{f,evap}$. Consequently, the liquid length, con-
 206 sidered as the maximum liquid-phase penetration, could be defined as the
 207 position on the spray axis where this specific $Y_{f,evap}$ is reached. Following
 208 this hypothesis, a scaling law for liquid length has been derived [24] based
 209 on turbulent spray mixing considerations. The axial mass fraction within the
 210 quasi-steady part of a diesel spray could be obtained from:

$$Y_f = K \cdot d_0 \sqrt{\frac{\rho_f}{\rho_{air}}} \cdot \frac{1}{X} \quad (1)$$

211 where K states for a spray constant, d_0 is nozzle diameter, ρ_f and ρ_{air} fuel
 212 and ambient density and X is spray axial coordinate. Thus, liquid length is
 213 defined by:

$$LL = K \cdot [d_0 \sqrt{\frac{\rho_f}{\rho_{air}}}] \cdot \frac{1}{Y_{f,evap}} \quad (2)$$

214 In Eqn. (2), the term in brackets is widely known in the literature as the
 215 equivalent diameter and is related to spray mixing scales (i.e momentum)
 216 while the last one, as stated before, is an energy term which takes into
 217 account vaporization processes. This last term could be written as in Eqn.
 218 (3), where T_{air} is ambient gas temperature, $T_{f,0}$ is the initial fuel temperature
 219 and T_{evap} is the saturation temperature when the fuel is fully vaporized.

$$\frac{1}{Y_{f,evap}} = 1 + \frac{\Delta h_f(T_{evap}, T_{f,0})}{\Delta h_{air}(T_{air}, T_{evap})} \quad (3)$$

220 This parameter shows a complex dependence on both fuel properties and
 221 ambient conditions [16, 24] such as air temperature, fuel specific and latent
 222 heat, and fuel initial temperature.

223 *3.2. Statistical analysis*

224 These theoretical considerations have been applied in a statistical study
225 in order to analyse experimental results and check hypotheses reliability.
226 This study aims at relating liquid length with operating conditions and fuel
227 characteristics. The following model for the dependence of liquid length has
228 been proposed:

$$LL \propto D_{noz}^a \cdot T_{air}^b \cdot P_{inj}^c \cdot \rho_{air}^d \cdot \rho_f^e \cdot \nu_f^f \cdot T_{10\%}^g \cdot T_{50\%}^h \cdot T_{95\%}^i \quad (4)$$

229 The classical correlations for liquid length in diesel sprays have been com-
230 pleted with some factors particular to the fuel so that fuel fluid-mechanical
231 and vaporizing properties are accounted. Coefficients b, c, d from Eqn. (4)
232 have been previously evaluated independently for each fuel under both steady
233 and unsteady conditions. Nozzle diameter effect has not been studied so
234 D_{noz}^a and will be consequently part of the constant factor. Injection pressure
235 exponent has been kept free, despite injection velocity (and thus injection
236 pressure) has theoretically no influence on liquid length.

237 *3.3. Steady-State Conditions Approach*

238 The assumption of steady-state conditions has already been made by the
239 authors in previous studies [12, 13] and so liquid length was considered to
240 be constant around engine *TDC* and resolve exponents from Eqn. (4) in
241 terms of average values. A window for time-averaging is selected on the
242 stabilized liquid-length region. The engine first-law thermodynamic analysis
243 showed that the engine reaches T_{max} between -2.8 and -3.1 °*ATDC* (4500
244 and 4625 μs *ASOE*) and ρ_{max} between -0.1 and -0.5 °*ATDC* (5500 and

245 5625 μs *ASOE*), depending on the engine operating conditions. Therefore,
246 time-averaging window has been limited between 3500 and 6500 μs *ASOE*.
247 Figure 8 shows a plot of the ensemble average and its standard deviation. The
248 section used for time-averaging has been highlighted and the result plotted
249 in dashed line. Images from one of the ten corresponding sequences have
250 been added for illustration. Only one image out of two has been displayed
251 to simplify the figure.

252 [Figure 8 about here.]

253 Only the most relevant results of this analysis have been plotted in the
254 Results and Discussion section but the whole set of numerical results is pro-
255 vided in an appendix table.

256 3.4. *In-Cylinder Unsteady Conditions Approach*

257 In order to check if both empirical models based on results obtained un-
258 der steady-state conditions and spray models based on a succession of quasi-
259 steady evaporating states [16, 19] are extendable to real engine conditions,
260 most of the image sequence has been exploited by attributing to each image
261 of the spray its corresponding couple of T_{air} and ρ_{air} and resolve Eqn. (4) in
262 terms of time-resolved values. As commented in the experimental apparatus
263 description, the spray is exposed to important pressure variations. On Fig-
264 ure 5, it can be observed how T_{air} fluctuates over more than 50 K and so does
265 ρ_{air} by up to 7 $kg.m^{-3}$ during the injection event ($\approx 24 CAD$). This is due
266 to the relative long injection timing (8 ms) compared to engine speed (500
267 rpm). Figure 8 shows how the in-cylinder pressure leaves its mark on the
268 ensemble-averaged liquid length. Temperature and density time-derivatives

269 have been plotted in Figure 9. It is worthy to note that despite the temporal
270 variations seem to be small, they are of the order of expected variations in a
271 heavy-duty engine at 1200 *rpm* in the injection region for *HCCI* combustion
272 mode and in the close-to-*TDC* region for a conventional combustion mode.
273 For this analysis, the time window used for analysis had also to be restricted
274 to avoid the consideration of *SOI* and *EOI* penetration transients. As an
275 example, the case exposed in Figure 8, has been restricted between 1375
276 and 8875 μs *ASOE*. The liquid length results have been reprocessed using
277 the same statistical method described above in order to assess the effect of
278 air temperature and air density. From a statistical point of view, such kind
279 of study is very interesting since it multiplies the combinations of T_{air} and
280 ρ_{air} . Moreover, blow-by, heat transfer and mechanical stresses induce a delay
281 between both traces and reduce collinearity between both variables.

282 [Figure 9 about here.]

283 4. Results and Discussion

284 [Figure 10 about here.]

285 4.1. Steady-State Conditions

286 The liquid length at different injection pressures has been plotted for
287 the five studied fuels in Figure 10. Significant differences can be observed
288 from one fuel to another given the reduction by more than a factor of two
289 between *RME* and *FT2* liquid lengths. Both of these fuels constructed
290 the upper and lower boundaries of the tested fuels, respectively. Figure 10
291 shows similar trends regarding two fuels encasing the others by upper and

292 lower boundaries as in Figure 1, which illustrates the high influence of fuel
293 volatility. Such result was then expected since the association between liq-
294 uid length and distillation curves is already widely assumed in the literature
295 [3, 10, 4]. The last works available on the subject still use this measurement
296 to explain both the shorter FTD liquid length [20] and the higher biodiesel
297 liquid length [21, 22] respective to the conventional diesel. A slight decrease
298 of the liquid length can be observed among all the fuels when injection pres-
299 sure is increased. However, this effect is small enough to consider this result
300 in agreement with the "mixing-controlled" assumption. Although only the
301 *NO*-condition is represented, the same trends have been observed for the
302 four other operating points. Since it has just been confirmed that injection
303 pressure had no considerable effect on liquid-phase penetration, the effects
304 of air temperature and air density have been represented only for the 150
305 *MPa* injection pressure case in Figures 11 and 12. Again, the fuel hierarchy
306 is conserved and is quite consistent with the distillation curves at ambient
307 pressure. For all fuels, an increase on both air parameters leads to a reduc-
308 tion of the liquid length. Likewise, the effect of T_{air} appears to be extremely
309 significant. Indeed, a 13% increase of air temperature affects up to a 43%
310 decrease on the liquid length, while a 36% increase of air density only de-
311 creases the liquid length by up to a 25%. It must be highlighted that the
312 100 *K* variation applied in this study is far from covering the whole range
313 of temperatures encountered in a diesel engine. Consequently, in early and
314 late injection strategies, where the ambient temperature is expected to be
315 even lower, the resulting liquid length, enhanced by the lower density as
316 well, could lead to an important liner-impingement if care is not taken dur-

317 ing the hardware design. The purpose of the following section is precisely to
318 assess the weight of these parameters by means of the previously described
319 statistical analysis.

320 [Figure 11 about here.]

321 [Figure 12 about here.]

322 4.2. Statistical regression for engine-depending physical processes assessment

323 In a first instance, the statistical analysis has been applied to each fuel
324 independently, introducing only the parameters which change with the oper-
325 ating settings of the engine. In this way it is pretended to check if all fuels
326 have the same sensitivity to engine parameters. T_{air} , ρ_{air} and P_{inj} effect
327 have been assessed and are presented in Table 5. Both temperature high
328 impact and injection pressure irrelevance are confirmed while air density ef-
329 fect seems to be a bit higher than proposed by the scaling law. Moreover,
330 from one fuel to the other, slight differences are appreciated, indicating a
331 difference on fuel response to engine thermodynamic settings. Indeed, RME
332 seems to be more gently affected by air conditions, way above the rest. If
333 results from steady and unsteady-state are now considered for comparison, it
334 can be observed that, exception made for RME , the resulting exponents are
335 remarkably close. It may be necessary to remind here that the "steady-state"
336 exponents have been obtained using a set of averaged data coming from a
337 sweep of three air density values at constant air temperature and from a
338 sweep of three air temperature values at constant air density, both fueled at
339 three injection pressures levels (15 values/fuel), while "unsteady state" con-
340 sideres air density and temperature values during the entire injection event

341 for both sweeps (≈ 900 values/fuel). This parallelism in the results shows
342 how a spray under unsteady conditions behaves as a succession of sprays ob-
343 tained under steady-state conditions, meaning that there is no delay in the
344 spray adjustment to its environment under the range of pressure derivatives
345 studied. This result is in agreement with recent studies [25] and validates
346 the use of theoretical 1D spray models [16, 19, 23] in unsteady conditions
347 as well as empirical models based on liquid length measurements obtained
348 in a steady-state environment. Such conclusions are supported by the high
349 correlations reliability that has been evaluated through the R-squared pa-
350 rameter which is, apart for *RME*, consistent between steady and unsteady
351 state conditions.

352 [Table 4 about here.]

353 The differences observed on exponents for *RME* as well as the decay
354 observed on R^2 show that this fuel may not follow the same conclusions
355 depicted above and that the characteristic time of vaporization for a droplet
356 of such a dense, viscous and low volatility fuel may be significant compared
357 to the spray flow field development. In [21], Fisher *et al.* performed a similar
358 analysis as in [25] but using two biodiesel fuels. They also observed that
359 biodiesel liquid length is not directly related to instantaneous in-cylinder
360 temperature and density, and suggest that biodiesel may be subject to the
361 thermodynamic history. An attempt has been made to quantify the biodiesel
362 time-response. However the quality of the result showed to be highly affected
363 by our relatively low camera frequency. Yet, no clear trends were found when
364 this delay was correlated either with engine parameters or with the proper

365 liquid length. Thus, both data and correlations were not robust enough to
366 be presented in this manuscript and more investigation on the subject will be
367 needed. Finally, liquid length results from all the fuels have been introduced
368 to the statistical analysis simultaneously. As expected, if no dramatic effect
369 can be observed on exponents' values, the very low R^2 shows that physical
370 parameters issued from the engine setup are not sufficient to predict liquid
371 length and that it is necessary to introduce fuel physical properties to achieve
372 a better prediction.

373 *4.3. Statistical regression for fuel physics assessment*

374 The same statistical tool has been applied, introducing data from the
375 measured fuel physical properties exposed in the upper corresponding sec-
376 tion. They have been separated in 2 parts: fluid-mechanics and evaporative
377 properties. Fluid-mechanics properties are represented by density and vis-
378 cosity while evaporative properties, in absence of specific and latent heat,
379 are represented by $T_{10\%}$, $T_{50\%}$ and $T_{95\%}$ from distillation curves. Indeed, the
380 purpose of the resulting correlations is to provide a tool that predicts liquid
381 length out of cheap, off-engine measurements. A set of selected correlations
382 are presented in Table 5 by using only some of the terms in Eqn. (4). In
383 order to compare correlations with a different number of parameters, reliabil-
384 ity has been calculated using specific R-squared (R_{spe}^2). As in the previous
385 section, no significative differences have been observed between steady and
386 unsteady-state considerations and therefore, only unsteady-state conditions
387 are reported in Table 6. First, physical properties issued from the engine
388 operation and fuel physical properties have been compared in correlations
389 (1) and (2). It appears that fuel properties are more important than physi-

390 cal in the prediction of liquid length. However negative coefficients for $T_{10\%}$
391 and $T_{95\%}$ are not physically reasonable. It is important then to identify,
392 among the five physical parameters, which are controlling the process. In
393 correlations (3) to (7), each fuel parameter has been associated to one phys-
394 ical parameters issue from the engine. Fuel density seems to be the best
395 parameter for liquid length prediction, while no significant differences can
396 be observed separating the 3 distillation curve temperatures. However the
397 low R^2 for $T_{95\%}$ is unacceptable. In correlations (8) and (9), the fuel fluid
398 mechanics properties and fuel evaporative properties are respectively asso-
399 ciated to engine physical properties. The result is that they are both good
400 groups of variables for empirical modelling, although, again, the negative
401 exponents for $T_{10\%}$ and $T_{95\%}$ are a physical non-sense. Finally, correlation
402 (10) shows the association of both fluid-mechanics and evaporative proper-
403 ties using the most essential and reliable parameters. Correlation (11) has
404 been added to show the maximum reliability these parameters are capable
405 of, for comparison with upper correlations.

406 [Table 5 about here.]

407 5. Summary and Conclusions

408 Measurements of the maximum liquid-phase penetration have been per-
409 formed using five fuels with an interesting potential for diesel substitution,
410 in an optical engine under a large set of thermodynamic and injection con-
411 ditions. These measurements have been related to fuel properties measure-
412 ments performed off-engine and to pressure variations similar to those found

413 in a heavy-duty diesel engine, in order to assess the physical processes control-
414 ling the vaporization of a spray under such conditions. Relevant conclusions
415 are the following:

- 416 1. A database of fuel properties and time-averaged liquid-length results
417 are provided for confrontation with modeling results (Cf. Appendix).
- 418 2. Under all tested conditions, Fischer-Tropsch fuels showed to have a
419 shorter liquid length than biodiesel fuels, for which the liquid length
420 was increased as the *RME* percentage was increased as well. The fuel
421 hierarchy for liquid length was the following: $FT2 < FT1 < B05 <$
422 $B30 < RME$. This trend was maintained for all engine settings.
- 423 3. The qualitative effects of T_{air} , ρ_{air} and P_{inj} already available in the
424 literature for diesel fuel have been confirmed and could be extended to
425 biodiesel and Fischer-Tropsch fuels.
- 426 4. A new method, based on time consideration, has been proposed for the
427 processing liquid length high speed imaging. It permitted to multiply
428 the number of samples for a more robust statistical analysis.
- 429 5. For 4 out of the 5 tested fuels, the comparison between two statistical
430 approaches showed that the spray liquid-phase adjust instantaneously
431 to the in-cylinder conditions. Such results confirms the hypothesis
432 made by 1D spray models and allows the use of empirical models ob-
433 tained under steady-state environment in unsteady conditions (with
434 time-derivatives up to $20000 K.s^{-1}$ and $2000 kg.m^{-3}.s^{-1}$).
- 435 6. Fuel physical properties have been assessed against the physical prop-
436 erties resulting from engine operating conditions and traduced into cor-
437 relations for empirical modeling.

438 7. A correlation based on low cost off-engine measurements is proposed
439 taking into account engine parameters, fuel fluid-mecanics properties
440 and evaporation properties: $LL = T_{air}^{-2.63} \cdot P_{inj}^{-0.06} \cdot \rho_{air}^{-0.60} \cdot \rho_f^{4.39} \cdot T_{50\%}^{0.54}$

441 **Acknowledgment**

442 The authors wish to acknowledge the Spanish Ministry of Education and
443 Science for the financial support through the OPTICOMB project (TRA2007-
444 67961-C03-01). The authors would also like to thank Daniel Lerida for the
445 management of the facility and his assistance in data acquisition.

446 [Table 6 about here.]

447 **Appendix**

Fuel	T_{air}	ρ_{air}	P_{inj}	ΔP	ρ_f	ν_f	$T_{10\%}$	$T_{50\%}$	$T_{95\%}$	LL
B05	798.0	29.7	50	43.2	833	2.50	205	293	356	19.34
	798.0	29.7	100	93.2	833	2.50	205	293	356	18.42
	798.0	29.7	150	143.2	833	2.50	205	293	356	16.87
	845.2	25.8	50	43.7	833	2.50	205	293	356	17.83
	845.2	25.8	100	93.7	833	2.50	205	293	356	16.55
	845.2	25.8	150	143.7	833	2.50	205	293	356	15.84
	795.4	21.7	50	45.1	833	2.50	205	293	356	24.01
	795.4	21.7	100	95.1	833	2.50	205	293	356	22.68
	795.4	21.7	150	145.1	833	2.50	205	293	356	21.42
	747.5	25.9	50	44.5	833	2.50	205	293	356	25.64

Continued on next page

Appendix – continued from previous page

Fuel	T_{air}	ρ_{air}	P_{inj}	ΔP	ρ_f	ν_f	$T_{10\%}$	$T_{50\%}$	$T_{95\%}$	LL
	747.5	25.9	100	94.5	833	2.50	205	293	356	24.87
	747.5	25.9	150	144.5	833	2.50	205	293	356	22.90
	796.8	25.8	50	44.1	833	2.50	205	293	356	22.05
	796.8	25.8	100	94.1	833	2.50	205	293	356	20.17
B05	796.8	25.8	150	144.1	833	2.50	205	293	356	19.07
B30	798.0	29.7	50	43.2	849	3.10	223	304	347	24.53
	798.0	29.7	100	93.2	849	3.10	223	304	347	26.15
	798.0	29.7	150	143.2	849	3.10	223	304	347	24.28
	845.2	25.8	50	43.7	849	3.10	223	304	347	24.16
	845.2	25.8	100	93.7	849	3.10	223	304	347	23.07
	845.2	25.8	150	143.7	849	3.10	223	304	347	20.48
	795.4	21.7	50	45.1	849	3.10	223	304	347	30.58
	795.4	21.7	100	95.1	849	3.10	223	304	347	31.86
	795.4	21.7	150	145.1	849	3.10	223	304	347	31.17
	747.5	25.9	50	44.5	849	3.10	223	304	347	30.93
	747.5	25.9	100	94.5	849	3.10	223	304	347	32.08
	747.5	25.9	150	144.5	849	3.10	223	304	347	33.41
	796.8	25.8	50	44.1	849	3.10	223	304	347	28.49
	796.8	25.8	100	94.1	849	3.10	223	304	347	27.80
B30	796.8	25.8	150	144.1	849	3.10	223	304	347	26.03
RME	798.0	29.7	50	43.2	878	4.41	321	334	345	31.67
	798.0	29.7	100	93.2	878	4.41	321	334	345	29.57

Continued on next page

Appendix – continued from previous page

Fuel	T_{air}	ρ_{air}	P_{inj}	ΔP	ρ_f	ν_f	$T_{10\%}$	$T_{50\%}$	$T_{95\%}$	LL
	798.0	29.7	150	143.2	878	4.41	321	334	345	30.20
	845.2	25.8	50	43.7	878	4.41	321	334	345	27.80
	845.2	25.8	100	93.7	878	4.41	321	334	345	27.57
	845.2	25.8	150	143.7	878	4.41	321	334	345	25.88
	795.4	21.7	50	45.1	878	4.41	321	334	345	39.14
	795.4	21.7	100	95.1	878	4.41	321	334	345	40.63
	795.4	21.7	150	145.1	878	4.41	321	334	345	39.36
	747.5	25.9	50	44.5	878	4.41	321	334	345	38.71
	747.5	25.9	100	94.5	878	4.41	321	334	345	45.85
	747.5	25.9	150	144.5	878	4.41	321	334	345	45.69
	796.8	25.8	50	44.1	878	4.41	321	334	345	36.73
	796.8	25.8	100	94.1	878	4.41	321	334	345	35.50
RME	796.8	25.8	150	144.1	878	4.41	321	334	345	34.03
FT1	798.0	29.7	50	43.2	784	3.44	250	297	352	18.26
	798.0	29.7	100	93.2	784	3.44	250	297	352	17.33
	798.0	29.7	150	143.2	784	3.44	250	297	352	16.12
	845.2	25.8	50	43.7	784	3.44	250	297	352	17.07
	845.2	25.8	100	93.7	784	3.44	250	297	352	15.90
	845.2	25.8	150	143.7	784	3.44	250	297	352	15.72
	795.4	21.7	50	45.1	784	3.44	250	297	352	22.31
	795.4	21.7	100	95.1	784	3.44	250	297	352	20.79
	795.4	21.7	150	145.1	784	3.44	250	297	352	20.08

Continued on next page

Appendix – continued from previous page

Fuel	T_{air}	ρ_{air}	P_{inj}	ΔP	ρ_f	ν_f	$T_{10\%}$	$T_{50\%}$	$T_{95\%}$	LL
	747.5	25.9	50	44.5	784	3.44	250	297	352	23.28
	747.5	25.9	100	94.5	784	3.44	250	297	352	22.22
	747.5	25.9	150	144.5	784	3.44	250	297	352	20.92
	796.8	25.8	50	44.1	784	3.44	250	297	352	19.53
	796.8	25.8	100	94.1	784	3.44	250	297	352	18.48
FT1	796.8	25.8	150	144.1	784	3.44	250	297	352	17.54
FT2	798.0	29.7	50	43.2	773	1.29	177	200	242	13.53
	798.0	29.7	100	93.2	773	1.29	177	200	242	13.09
	798.0	29.7	150	143.2	773	1.29	177	200	242	12.15
	845.2	25.8	50	43.7	773	1.29	177	200	242	13.08
	845.2	25.8	100	93.7	773	1.29	177	200	242	12.36
	845.2	25.8	150	143.7	773	1.29	177	200	242	11.70
	795.4	21.7	50	45.1	773	1.29	177	200	242	16.69
	795.4	21.7	100	95.1	773	1.29	177	200	242	15.92
	795.4	21.7	150	145.1	773	1.29	177	200	242	15.58
	747.5	25.9	50	44.5	773	1.29	177	200	242	18.75
	747.5	25.9	100	94.5	773	1.29	177	200	242	16.92
	747.5	25.9	150	144.5	773	1.29	177	200	242	15.94
	796.8	25.8	50	44.1	773	1.29	177	200	242	15.21
	796.8	25.8	100	94.1	773	1.29	177	200	242	13.77
FT2	796.8	25.8	150	144.1	773	1.29	177	200	242	13.37

449 **References**

- 450 [1] Browne KR, Partridge IM, Greeves G. Fuel Property Effects on Fuel/Air
451 Mixing in an Experimental Diesel Engine. SAE Paper 860233; 1986
- 452 [2] Verhoeven D, Vanhemelryck JL, Baritaud T. Macroscopic and Ignition
453 Characteristics of High-Pressures Sprays of Single-Component Fuels.
454 SAE Paper 981069; 1998
- 455 [3] Canaan RE, Dec JE, Green RM, Daly DT. The Influence of Fuel Volatil-
456 ity on the Liquid-Phase Fuel Penetration in a Heavy-Duty D.I. Diesel
457 Engine. SAE Paper 980510; 1998
- 458 [4] Higgins BS, Mueller CJ, Siebers D. Measurements of Fuel Effects on
459 Liquid-Phase Penetration in DI Sprays, SAE Paper 1999-01-0519; 1999
- 460 [5] Official Journal of the European Union, Directive 2003/30/EC of the
461 European parliament and of the council of 8 May 2003 on the promotion
462 of the use of biofuels or other renewable fuels for transport.
- 463 [6] Beatrice C, Guido C, Di Iorio S. Experimental analysis of alternative fuel
464 impact on a new torque-controlled light-duty diesel engine for passenger
465 cars. Fuel, 89:32783286; 2010
- 466 [7] Bermúdez V, García JM, Juliá E, Martínez S. Engine with Optically
467 Accessible Cylinder Head: a Research Tool for Injection and Combustion
468 Processes. SAE Paper 2003-01-1110; 2003
- 469 [8] Design and Operation of a High Pressure, High Temperature Cell for HD
470 Diesel Spray Diagnostics: Guidelines and Results. Baert RSG, Frijters

- 471 PJM, Somers B, Luijten CCM, de Boer W. SAE Paper 2009-01-0649;
472 2009
- 473 [9] Dec JE, Espey C. The Effect of Tdc Temperature and Density on the
474 Liquid-Phase Fuel Penetration in a D.I. Diesel Engine. SAE Trans.,
475 104(4):1400-1414; 1995
- 476 [10] Siebers DL. Liquid-Phase Fuel Penetration in diesel Sprays, SAE Trans.,
477 107(3):1205-1227; 1998
- 478 [11] Payri R, Salvador FJ, Gimeno J, Zapata LD. Diesel nozzle geometry in-
479 fluence on spray liquid-phase fuel penetration in evaporative conditions.
480 Fuel,87(7):1165-1176; 2008
- 481 [12] Pastor JV, Pastor JM, Gimeno J, Nerva J-G. The effect of Biodiesel
482 fuel blend rate on the Liquid-phase fuel penetration in Diesel engine
483 conditions, SAE Paper 2009-24-0051; 2009
- 484 [13] Pastor JV, Payri R, Gimeno J, Nerva J-G. Experimental Study on RME
485 Blends: Liquid-Phase Fuel Penetration, Chemiluminescence, and Soot
486 Luminosity in Diesel-Like Conditions. Energy Fuels, 23(12):5899-5915;
487 2009
- 488 [14] Klein-Douwel RJH, Frijters PJM, Somers LMT, de Boer WA, Baert
489 RSG. Macroscopic diesel fuel spray shadowgraphy using high speed dig-
490 ital imaging in a high pressure cell. Fuel 86:19942007; 2007
- 491 [15] Allocca L, Mancaruso E, Montanaro A, Sequino L, Vaglietto BM. Ef-
492 fects of mineral and biodiesel fuel compositions on spray evolution and
493 mixture distribution. THIESEL Conference. Valencia, Spain; 2010

- 494 [16] Siebers DL. Scaling Liquid-Phase Fuel Penetration in diesel Sprays
495 Based on Mixing - Limited Vaporization, SAE Trans., 108(3):703-728;
496 1999
- 497 [17] Pastor JV, Arrègle J, Palomares A. Diesel spray image segmentation
498 with a likelihood ratio test. Applied Optics, 40:1-10; 2001
- 499 [18] Pastor JV, Arrègle J, García JM, Zapata LD. Segmentation of Diesel
500 spray images with loglikelihood ratio test algorithm for non-Gaussian
501 distributions. Applied Optics, 46(6):888-899; 2007
- 502 [19] Pastor JV, López JJ, García JM, Pastor JM. A 1D model for the descrip-
503 tion of mixing-controlled inert diesel sprays. Fuel, 87(13-14):2871-2885;
504 2008
- 505 [20] Azimov U, Kim KS. Visualization of Gas-to-Liquid (GTL) Fuel Liq-
506 uid Length and Soot Formation in the Constant Volume Combustion
507 Chamber. Journal of Thermal Science and Technology, 3:461-473; 2008
- 508 [21] Fisher BT, Knothe G, Mueller CJ. Liquid-Phase Penetration under Un-
509 steady In-Cylinder Conditions: Soy- and Cuphea-Derived Biodiesel Fu-
510 els Versus Conventional Diesel. Energy Fuels, 24:51635180; 2010
- 511 [22] Genzale CL, Pickett LM, Kook S, Liquid Penetration of Diesel and
512 Biodiesel Sprays at Late-Cycle Post-Injection Conditions. SAE Paper
513 2010-01-0610; 2010
- 514 [23] Musculus MPB, Kattke K. Entrainment Waves in Diesel Jets, SAE Int.
515 J. Engines 2:1170-1193; 2009

- 516 [24] Desantes JM, Pastor JV, Payri R, Pastor JM. Experimental character-
517 ization of internal nozzle flow and diesel spray behavior. Part II. Evap-
518 orative conditions. *Atomization and Sprays*, 15:517-543; 2005
- 519 [25] Fisher BT, Mueller CJ. Liquid penetration length of heptamethyl-
520 nonane and trimethylpentane under unsteady in-cylinder conditions.
521 *Fuel*, 89:2673-96; 2010

List of Figures

1	Distillation curves obtained by <i>ASTM D86</i>	30
2	Temperature effect on fuel density under atmospheric pressure.	31
3	Hot spray test rig and diffuse back-lightening optical setup.	32
4	Cutaway view of the injector tip.	33
5	Schematic representation of the engine operating conditions.	34
6	Results of in-cylinder first-law thermodynamic analysis for temperature and density calculation in the <i>TDC</i> region. 8 <i>ms</i> energizing time is represented by the injector current.	35
7	Intermediate processing images from FT2 at BT and $P_{inj}=100$ <i>MPa</i> . (a) Resulting image from original image subtraction to the background. (b) Overlay of the boundary resulting from the complete processing to the original image.	36
8	Representation of the cycle-to-cycle averaging and standard deviation (from 10 repetitions) for <i>FT1</i> , Low Density (22 kg.m^{-3} ; 800 <i>K</i>) at 50 <i>MPa</i> injection pressure. Images (1 out of 2) from one cycle have been added for illustration. The time-averaging window (3500 to 6500 $\mu\text{s ASOE}$) is represented in green and the time-averaged value dashed blue line. $\rho_{air}(t)$ and $T_{air}(t)$ are represented in the upper part of the figure.	37
9	Temperature and density time-derivatives during the injection event.	38
10	Injection pressure effect on liquid length for the five studied fuels at NO air conditions.	39
11	Air density effect on liquid length for the five studied fuels at 150 <i>MPa</i> injection pressure.	40
12	Air temperature effect on liquid length for the five studied fuels at 150 <i>MPa</i> injection pressure.	41

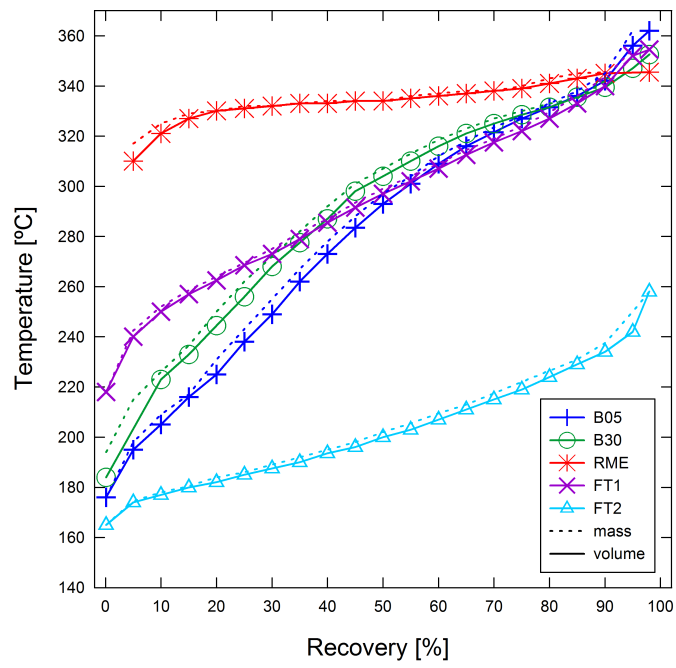


Figure 1: Distillation curves obtained by *ASTM D86*.

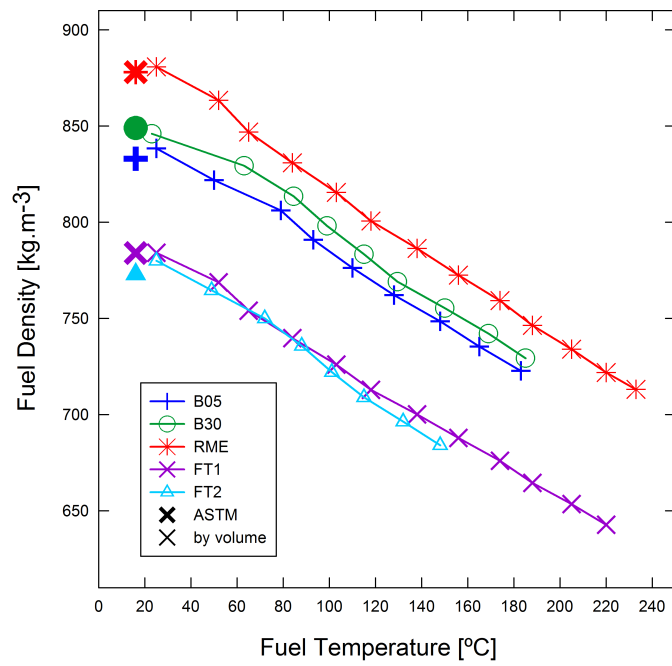


Figure 2: Temperature effect on fuel density under atmospheric pressure.

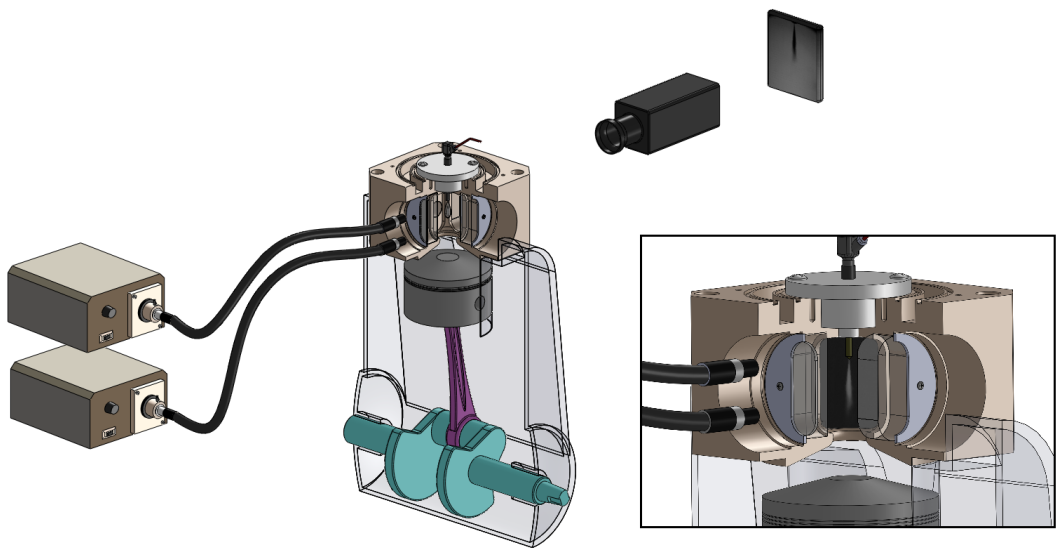


Figure 3: Hot spray test rig and diffuse back-lightening optical setup.

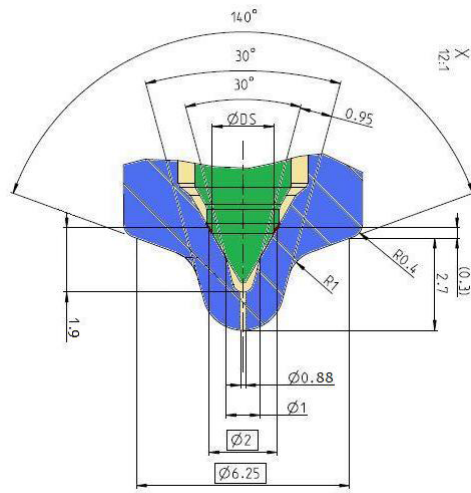


Figure 4: Cutaway view of the injector tip.

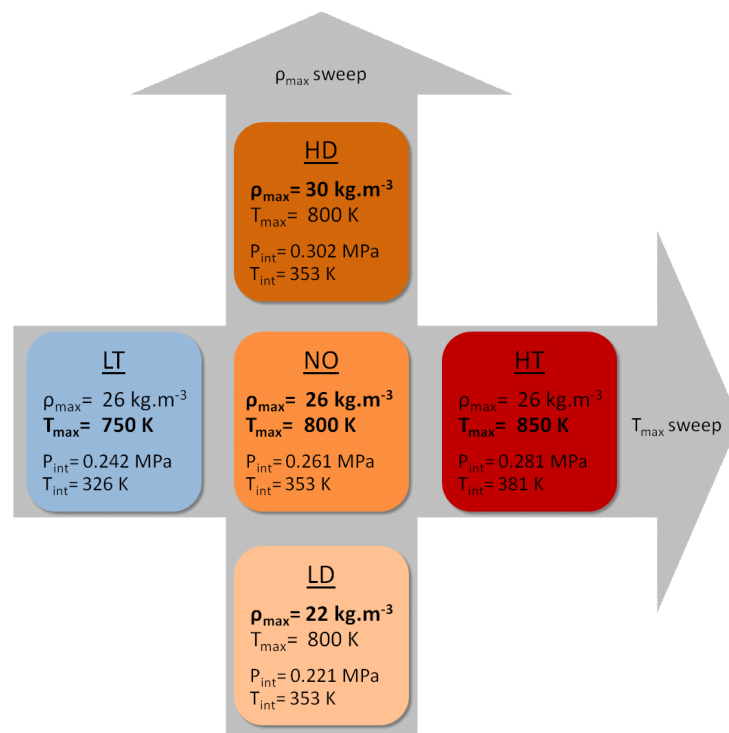


Figure 5: Schematic representation of the engine operating conditions.

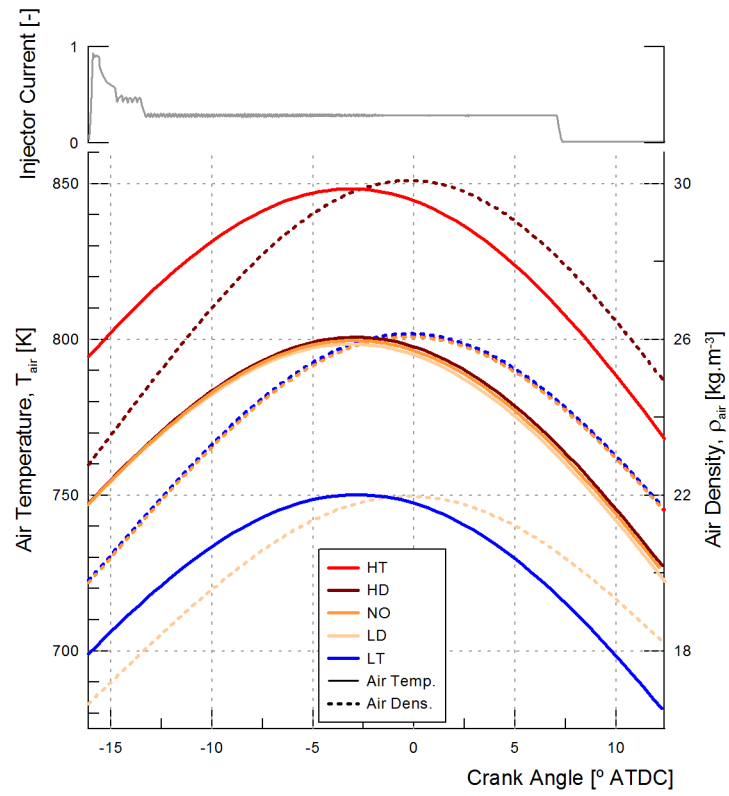


Figure 6: Results of in-cylinder first-law thermodynamic analysis for temperature and density calculation in the *TDC* region. 8 ms energizing time is represented by the injector current.

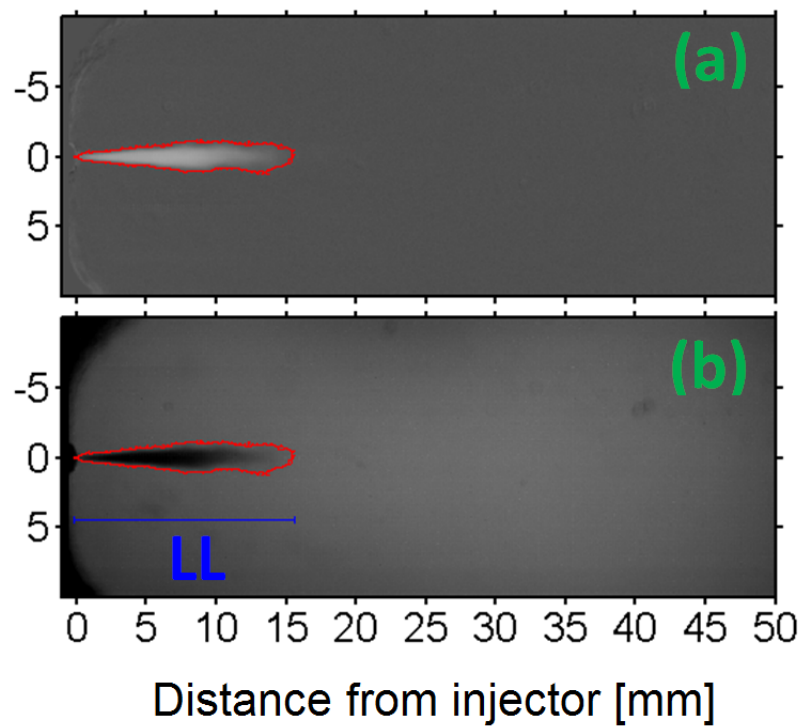


Figure 7: Intermediate processing images from FT2 at BT and $P_{inj}=100$ MPa. (a) Resulting image from original image subtraction to the background. (b) Overlay of the boundary resulting from the complete processing to the original image.

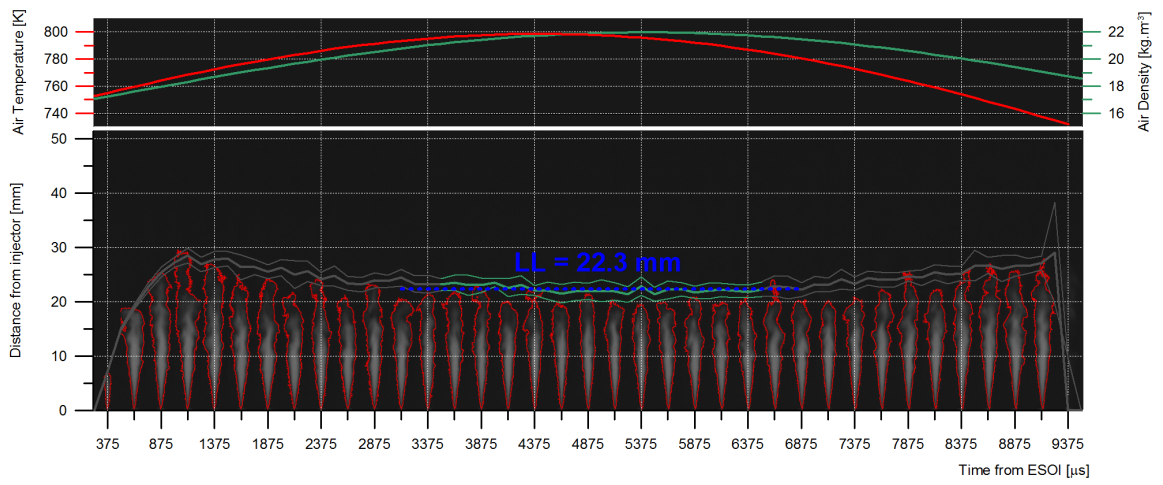


Figure 8: Representation of the cycle-to-cycle averaging and standard deviation (from 10 repetitions) for *FT1*, Low Density (22 kg.m^{-3} ; 800 K) at 50 MPa injection pressure. Images (1 out of 2) from one cycle have been added for illustration. The time-averaging window (3500 to 6500 $\mu\text{s ASOE}$) is represented in green and the time-averaged value dashed blue line. $\rho_{air}(t)$ and $T_{air}(t)$ are represented in the upper part of the figure.

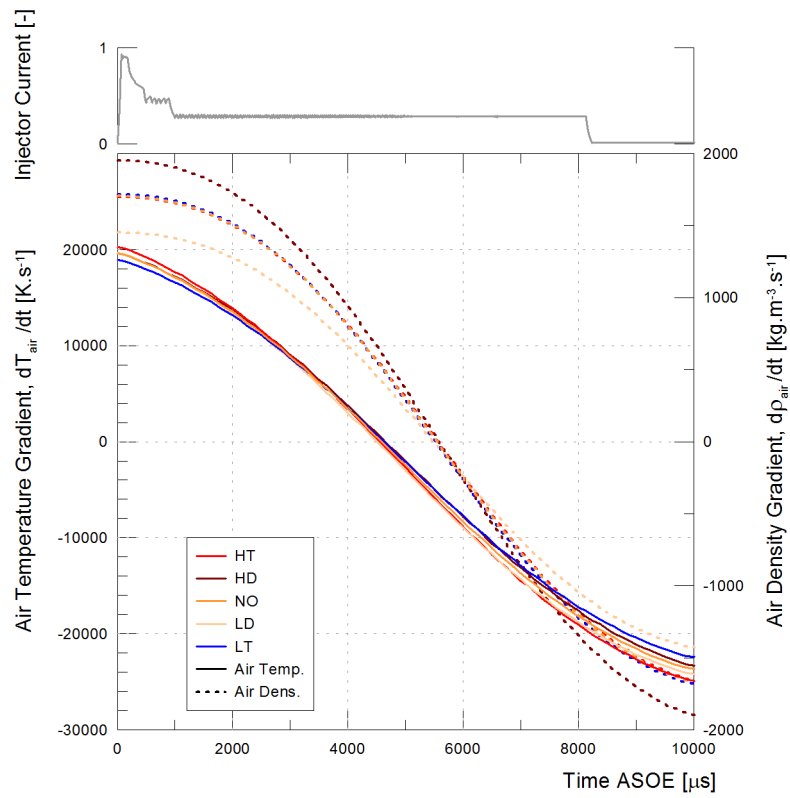


Figure 9: Temperature and density time-derivatives during the injection event.

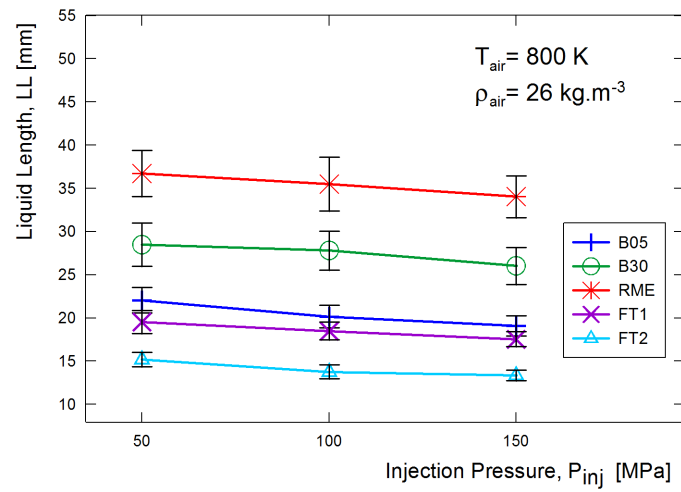


Figure 10: Injection pressure effect on liquid length for the five studied fuels at NO air conditions.

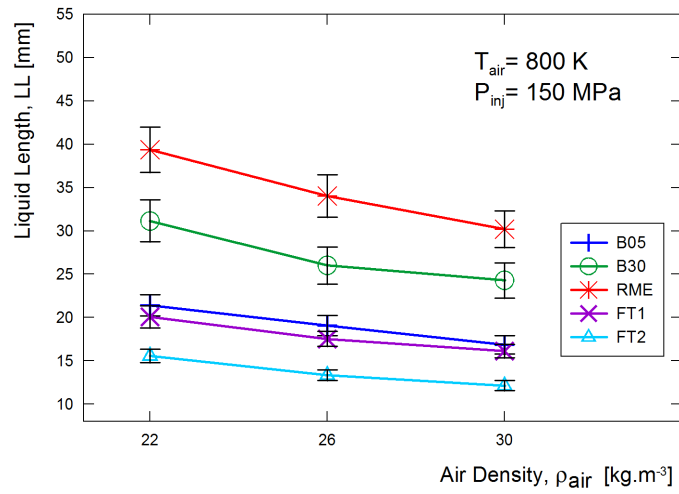


Figure 11: Air density effect on liquid length for the five studied fuels at 150 MPa injection pressure.

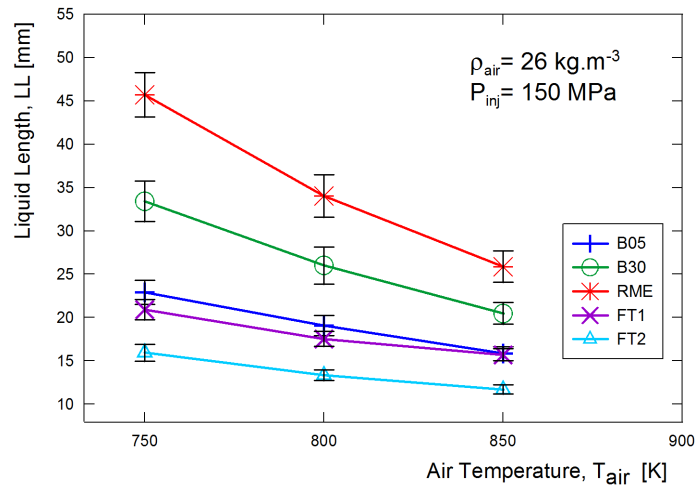


Figure 12: Air temperature effect on liquid length for the five studied fuels at 150 MPa injection pressure.

List of Tables

2	Fuel relevant properties.	43
3	Linear regression coefficients for fuel density dependency to temperature ($\rho_f = B + A.T_f$).	44
4	Injector characteristics.	45
5	Results from the statistical analysis for assessment of engine physical conditions under both steady and unsteady-conditions. Non-significative exponents (p-value>0.05) appear in grey. . .	46
6	Results from the statistical analysis for assessment of engine physical conditions and fuel physical properties under unsteady-state conditions.	47
7	Nomenclature	48

Table 2: Fuel relevant properties.

Fuels Properties	<i>Unit</i>	<i>ASTM Std.</i>	B05	B30	RME	FT1	FT2
Density	[$kg.m^{-3}$]	<i>D1298</i>	833	849	878	784	773
Kinematic Viscosity	[$mm^2.s^{-1}$]	<i>D445</i>	2.5	3.1	4.4	3.4	1.3
Lower Heating Value	[$MJ.kg^{-1}$]	<i>D240</i>	42.11	41.77	38.24	44.76	44.24
Equivalent Chemical Formula	-	<i>D5291</i>	-	-	$C_{18.95}H_{35.2}O_2$	$C_{17}H_{35.5}$	$C_{12}H_{25}O_{0.2}$
C/H ratio	-	-	-	-	0.538	0.479	0.480
A/F_{st} (20.9% XO_2)	-	-	-	-	12.398	14.748	14.388

Table 3: Linear regression coefficients for fuel density dependency to temperature ($\rho_f = B + A.T_f$).

Coefficients	B05	B30	RME	FT1	FT2
A	-0.747	-0.759	-0.815	-0.726	-0.804
B	859.5	871.2	900.6	801.8	803.6
R^2	99.8%	99.4%	99.8%	99.8%	99.4%

Table 4: Injector characteristics.

Injector	
Injector Type	Bosch Solenoid
Nozzle Type	Mini-Sac & Single Hole
Nozzle Diameter (Nominal/Measured)	80/82 μm
Nozzle Conicity	K 1.5
Energizing duration	8 <i>ms</i>
Injection pressures	50, 100, 150 MPa

Table 5: Results from the statistical analysis for assessment of engine physical conditions under both steady and unsteady-conditions. Non-significative exponents (p-value>0.05) appear in grey.

Parameter		Cte	d_0	T_{air}	P_{inj}	ρ_{air}	-	-
Exponents		-	a	b	c	d	R^2	RMSE
Theoretical		-	1	-1.58	0	-0.5	-	-
B05	<i>Steady-State</i>	3.0324E+11	-	-3.11	-0.10	-0.68	99.0	0.28
B30		3.7266E+10	-	-2.80	-0.02	-0.70	92.6	0.91
RME		3.2664E+15	-	-4.39	-0.04	-0.82	99.0	0.59
FT1		5.3889E+09	-	-2.55	-0.09	-0.63	99.3	0.19
FT2		1.1733E+10	-	-2.68	-0.10	-0.67	97.9	0.26
All fuels		1.2095E+11	-	-2.98	-0.06	-0.69	15.3	6.95
B05	<i>Unsteady-State</i>	3.0139E+11	-	-3.12	-0.10	-0.66	96.5	0.60
B30		3.9238E+10	-	-2.81	-0.02	-0.69	89.4	1.23
RME		7.9248E+12	-	-3.55	-0.01	-0.75	88.9	2.02
FT1		4.4816E+09	-	-2.54	-0.09	-0.60	97.4	0.43
FT2		3.1336E+09	-	-2.53	-0.09	-0.58	95.5	0.44
All fuels		9.9393E+08	-	-2.42	-0.05	-0.39	11.3	6.82

Table 6: Results from the statistical analysis for assessment of engine physical conditions and fuel physical properties under unsteady-state conditions.

Parameter		Cte	d_0	T_{air}	P_{inj}	ρ_{air}	ρ_f	ν_f	$T_{10\%}$	$T_{50\%}$	$T_{95\%}$	-	-	
Exponents	#	-	a	b	c	d	e	f	g	h	i	R_{spe}^2	RMSE	
Theoretical		-	1	-1.58	0	-0.5	0.5	-	-	-	-	-	-	
All fuels	<i>Unsteady-State</i>	(1)	9.9393E+08	-	-2.42	-0.05	-0.39	-	-	-	-	-	11.3	6.82
		(2)	1.0000E+00	-	-	-	-	0.71	0.22	-1.14	5.41	-4.53	78.2	3.45
		(3)	8.2699E-08	-	-2.78	-0.06	-0.61	5.99	-	-	-	-	88.7	2.57
		(4)	6.8209E+09	-	-2.72	-0.06	-0.55	-	0.62	-	-	-	79.5	3.15
		(5)	9.4517E+06	-	-2.68	-0.06	-0.54	-	-	1.27	-	-	75.1	3.80
		(6)	3.2668E+06	-	-2.66	-0.06	-0.54	-	-	-	1.39	-	69.0	4.10
		(7)	1.5327E+06	-	-2.51	-0.06	-0.47	-	-	-	-	1.27	45.4	5.01
		(8)	2.2874E-03	-	-2.74	-0.06	-0.61	4.39	0.26	-	-	-	94.6	1.62
		(9)	1.8131E+10	-	-2.85	-0.07	-0.63	-	-	-1.23	6.94	-5.45	97.9	0.97
		(10)	6.1213E-05	-	-2.63	-0.06	-0.60	4.39	-	-	0.54	-	94.4	1.57
		(11)	1.0000E+00	-	-2.85	-0.07	-0.63	6.61	1.70	-0.90	-2.89	-0.06	98.1	0.93

Table 7: Nomenclature

B05/B30	Fossil diesel with 5%/30% RME (in mass)
RME	Rapeseed Methyl-Ester
FT(D)	Fischer-Tropsch (Diesel)
LD/HD	Low/High Density condition (at 800 K)
LT/HT	Low/High Temperature condition (at 26 $kg.m^{-3}$)
NO	Nominal condition
OC	Operating Conditions
<i>Subscripts</i>	
0	relative to initial conditions
f	fuel
air	relative to the air surrounding the spray
inj	injection
max	maximum
evap	evaporation
back	relative to the spray counter-pressure
<i>Abbreviations</i>	
P	pressure
ΔP	pressure drop= $P_{inj} - P_{back}$
T	temperature
ρ	density
h	enthalpy
K	constant value
X	spray axis
Y	mixture fraction
LL	Liquid Length
1D	One-dimensional
(A)SOI/E, EOI	(after) start of injection/energizing, end of injection
(A)TDC	(After) Top Dead Center
ASTM	American society for testing and materials
CAD	crank angle degree
CFD	computational fluid dynamics
CMOS	complementary metal-oxide semiconductor
EGR	Exhaust Gas Recirculation
FID	flame ionization detector
HCCI	homogeneous charge compression ignition
LHV	Lower Heating Value [$MJ.kg^{-1}$]
NO_x	mono-nitrogen oxides
PM	particulate Matter
rpm	revolutions per minute
$R_{(spe)}^2$	(specific) coefficient of determination
RMSE	root mean square error
TTL	transistor-transistor logic